

Shock-induced volume-collapse phase transition in a Ce-La alloy dynamically compressed up to 20 GPa

Yun-Jun Gu^{1,*}, Kai Zhao^{2,*}, Hao Liu³, Guo-Jun Li⁴, Zhao-Qi Wang⁵, and Qi-Feng Chen^{6,†}

¹National Key Laboratory for Shock Wave and Detonation Physics, Institute of Fluid Physics, CAEP, Mianyang 621900, China

²School of Mechanical Engineering, Jiangnan University, Wuxi 214122, China

³School of Physics and Electronics, Hunan University, Changsha 410082, China

⁴School of Physics, Henan Normal University, Xinxiang 453007, China

⁵College of Science, Xi'an University of Science and Technology, Xi'an 710054, China

⁶School of Science, Southwest University of Science and Technology, Mianyang 621010, China



(Received 24 May 2023; revised 27 September 2023; accepted 28 September 2023; published 16 October 2023)

Understanding the complex multiphase properties of Ce and its alloys remains a long-standing scientific challenge. Here, we report experimental observations of the shock responses of Ce-5wt. %La alloy dynamically compressed up to 20 GPa using plate-impact shock experiments. The Ce-5wt. %La alloy is observed to undergo a volume collapse phase transition (PT) from the γ to the α phase with a volume change of $\sim 20\%$ and the shock-compression PT region is found to be between 0.997 and 4.835 GPa. Thermodynamic analysis shows that the few La additives markedly elevate the PT threshold pressure of Ce. The obtained experimental $P - V$ and $u_s - u_p$ results confirm the validity of the law of additive volumes for ideal mixtures for Ce-5wt. %La in an experimental pressure range from the α phase to the liquid phase. These data and observations can provide a better understanding of the multiphase properties of dynamically compressed Ce and its alloys, and have potential industrial applications in the synthesis of new materials at high pressures.

DOI: [10.1103/PhysRevB.108.144105](https://doi.org/10.1103/PhysRevB.108.144105)

I. INTRODUCTION

Accurate knowledge of the thermodynamical behavior of materials under dynamic compression is of significance in fundamental science and engineering applications [1–4], making an examination of the dynamic responses and related physical properties of materials of interest a high priority. The rare earth element Ce has received considerable attentions from the scientific community due to its complex phase diagram and phase transition (PT) dynamics [3,5–9]. Among the PTs between the seven allotropic phases (α , β , γ , δ , α' , α'' , ϵ) of Ce currently distinguished, the most well-known is the $\gamma \rightarrow \alpha$ isostructural PT, which is accompanied by a drastic volume change (up to 16.5%) [10]. Numerous studies have been dedicated to clarifying the underlying mechanisms of this unusual low-stress isostructural volume collapse PT via both theoretical modeling and experiments [7,11–13]. As explained by Nikolaev and Tsvyashchenko [9], the list of historical theoretical models for the $\gamma \rightarrow \alpha$ PT can be given as: (1) The promotional model, which suggests that the localized (core-level-like) f electron becomes itinerant (valencelike) while the $\gamma \rightarrow \alpha$ PT occurs, i.e., the electronic configuration follows the transition (γ -Ce) $4f^15d^16s^2 \rightarrow 4f^05d^26s^2$ (α -Ce). However, this model is not supported by the results of positron-annihilation experiments [14,15], Compton scattering [16], inelastic neutron scattering [17,18],

or density functional theory (DFT) calculations [19], in which almost no change in the $4f$ occupancy is observed. (2) The orbital-selective Mott-like (localization-delocalization) transition within the Hubbard model [20], which assumes that the number of $4f$ electrons remains constant upon the $\gamma \rightarrow \alpha$ PT, but their features change from localized in the γ phase to itinerant in the α phase. The physics of this model is thus dictated by the balance between the on-site Coulomb repulsion energy U and the $4f$ bandwidth W , i.e., the ratio U/W . Although U and W can be deduced from photoemission and inverse photoemission experiments [9,20], the determination of these two parameters is still ambiguous and challenging. (3) The Kondo volume collapse (KVC) model [21,22], which hypothesizes that the $4f$ electron stays localized in both the γ and α phases, but its interaction with band electrons at the Fermi level is more intense in the α phase. Furthermore, the Kondo hybridization between the $4f$ electron and the conducting valence electrons varies with the volume change during the PT process. Recently, Zhu *et al.* [13] studied the $\gamma \rightarrow \alpha$ PT in single crystalline Ce thin films by using angle-resolved photoemission spectroscopy (ARPES) measurements and DFT calculations. Their results showed that the change in the $f - c$ hybridization correlates with the suppression of the $\gamma \rightarrow \alpha$ PT, and were thus consistent with the scenario of the KVC model. However, the ARPES measurements carried out by Wu *et al.* [23] suggested that the Kondo and Mott mechanisms can coexist (or even act cooperatively) to give rise to an intriguing electronic phase with coherent $4f$ quasiparticle bands, agreeing well with itinerant $4f$ calculations and exhibiting unusual temperature dependence.

*These authors contributed equally to this work.

†chenqf01@gmail.com

Shock-wave experiments are well suited to the examination of high-pressure PT and can provide essential information for evaluating and checking the validity of theoretical models. Such experiments have been widely applied to measure high-pressure equations of state (EOS) [1,2,4,24–29], PT [5–8,11,30–32], and other dynamic processes [33,34]. However, for metals and alloys with complex PT behaviors under low and moderate shock pressures, it is difficult to experimentally study their dynamical multiphase properties, and locating phase boundaries and obtaining Hugoniot data for relevant phases remains a scientific challenge. A series of shock compression experiments have been performed, mainly aiming at the unusual and interesting high-pressure behavior of Ce including the low-stress isostructural volume collapse PT from γ to α [7,11] and moderate-pressure shock melting [3,8]. These experiments have provided essential information for understanding the multiphase behaviors of Ce and constructing its multiphase EOS.

Compared to pure elemental Ce, Ce-based alloys with few element additives can have much richer phase diagrams, enabling novel physics to be observed. Among the Ce-based alloys, Ce-La alloys are the main components of a “Mischmetal” mixture of rare earth elements making up the negative electrode in nickel metal hydride batteries, which has attracted upsurging interests for its applications in electronic components and “green” technologies [35–37]. In addition, Ce and La are neighbors in the periodic table and they have approximately equal atomic volumes, melting points, and boiling points, which provide a unique opportunity for creating a continuous series of ideal solid solutions [38] and investigating the effects of alloy additions on the thermodynamic behavior of a Ce matrix. Furthermore, a Ce-La alloy with a 5 wt. % of La additives (Ce-5wt. %La) is found to have similar bulk properties and phase transformation features to heavy actinide series materials with a few atomic percent additives. It can thus be considered as a surrogate for the latter [39] because of their similarity. The study of Ce-5wt. %La is therefore expected to provide valuable information for understanding the PT kinetics and related physical properties of the heavy actinide series materials and developing reliable theoretical models. Knowledge of the thermodynamic behavior of a dynamically compressed Ce-La alloy is not only of theoretical significance but is also very valuable for examining the shock response of this alloy. Up until now, however, shock compression data have only been made available for pure Ce and La [3,5–8,11,33,40,41]. For Ce-La alloys, experimental and theoretical results under pressure are limited to static compression at room temperature [42,43] and no shock-wave data have been reported in the literature. Thus, there exists an unexplored “blank” in their shock compression properties. Therefore, in order to examine the shock response of dynamically compressed Ce-5wt. %La alloy at low and moderate shock pressures, in this work, we design and perform plate-impact shock compression experiments using a high-performance powder gun shock wave generating facility coupled with a laser-interferometry velocity measurement system. The experiments enable us to obtain the shock Hugoniot of the Ce-5wt. %La alloy, observe a shock-induced volume collapse PT at low pressure, locate its shock-compression PT regime, and examine the effects of a

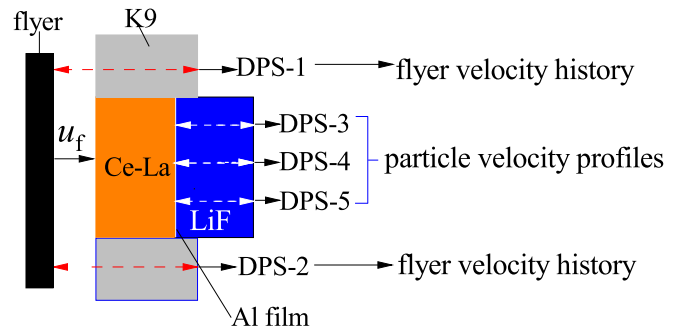


FIG. 1. A schematic experimental configuration. The flyer is accelerated by the $\phi 37$ powder gun facility and then impacts the Ce-La at a velocity of u_f to produce a shock wave to compress the sample to the desired Hugoniot states. Velocity histories are measured by multiple DPS probes. Probes DPS-1 and DPS-2 are used to measure the flyer velocity history through the K9 glass and Probes DPS-3, -4, and -5 are used to measure the particle velocity profile at the sample-LiF interface through the LiF optical window using Al film as a reflector.

few La additives on the thermodynamic behavior of Ce. The newly obtained experimental data can provide essential information for understanding the PT kinetics of such Ce-based alloys under shock compression, developing the multiphase EOS, and synthesizing new materials at high pressures.

II. EXPERIMENTAL METHODS

Plate-impact experiments for examining the shock response of dynamically compressed Ce-5wt. %La alloy were performed with a high-performance $\phi 37$ -mm-diameter powder gun facility together with velocity profile measurements. Figure 1 schematically shows the experimental configuration, which mainly consists of a flyer backed by a Ce-5wt. %La sample and a LiF optical window with a $\sim 10 \mu\text{m}$ thickness Al film. The Ce-5wt. %La sample and LiF window were embedded in an annulation made of transparent K9 glass. The Ce-5wt. %La sample has a measured initial density of $6.693 \pm 0.011 \text{ g/cm}^3$ and an ambient longitudinal sound velocity of $2.368 \pm 0.020 \text{ km/s}$. The flyer was accelerated by the powder gun facility and then impacted the left surface of the Ce-5wt. %La. Consequently, a strong shock wave was produced and compressed the sample up to the desired Hugoniot states. In the low-pressure regime, for dynamically compressed Ce, a two-wave structure was previously observed from measured velocity profiles when a shock-induced PT took place [7]. We expected such a two-wave structure to appear for the shock-compressed Ce-5wt. %La alloy at low pressure. Thus, in order to produce the desired single- and two-wave loading conditions, materials with three different shock impedances, copper (Cu), 2024 aluminum (2024Al), and Plexiglas (PMMA), were used to manufacture the flyer. Figure 2 schematically shows the wave propagation in Lagrangian space-time coordinates and the corresponding particle velocity profile at the sample-LiF interface, indicating the wave interactions in the sample upon two different loading conditions (Case 1 for two-wave loading and Case 2 for single-wave loading).

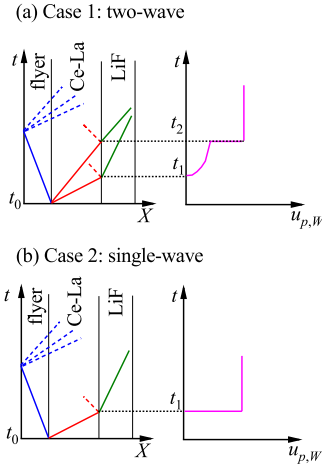


FIG. 2. Wave propagation in Lagrangian space-time coordinates and the corresponding particle velocity profile at the sample-LiF interface under two loading cases. (a) The wave propagation and particle velocity profile in the two-wave loading case. (b) The wave propagation and particle velocity profile in the single-wave loading case. The flyer impacts the sample at time t_0 . In the two-wave loading case, the two waves arrive at the sample-LiF interface at times t_1 and t_2 , respectively. In the single-wave loading case, the shock wave arrives at the sample-LiF interface at time t_1 .

The velocity histories were measured using a Doppler-pins-system (DPS) velocity interferometer with an operating wavelength of 1550 nm. In order to improve the measurement accuracy, multiple DPS probes located at different positions were used so that the effects of impact tilting could be corrected when determining the wave transit time in the sample (see Figure 1). By assembling the LiF optical window and transparent K9 glass as shown in Fig. 1, the velocity measurements enabled us to track the velocity evolution of the flyer and record the shock history in the sample and LiF window in a single shot. Figure 3 shows typical measurement signals detected by the DPS in two shots (shots 3 and 5) under different loading conditions. Using the plate-impact shock compression technique, we successfully realized both single- and two-wave loading conditions for the Ce-5wt. %La alloy, as can be clearly observed from the measured particle velocity profiles at the sample-LiF interface. The velocity measurements provided essential information on the flyer impact velocity, u_f , the particle velocity at the sample-LiF interface, $u_{p,w}$, and the wave transit time in the sample, Δt . Then, the Lagrangian wave velocity in the sample, u_s , could be determined from the measured transit time for the shock to traverse the sample, i.e., $u_s = d_0/\Delta t$, where d_0 is the initial thickness of the sample. Note that for two-wave loading (shot 5), two wave velocities were obtained as $u_{s,P1} = d_0/\Delta t_1$ for the P1 wave and $u_{s,P2} = d_0/\Delta t_2$ for the P2 wave, where $\Delta t_1 = t_1 - t_0$ and $\Delta t_2 = t_2 - t_0$ are the wave transit times of the P1 and P2 waves in the sample, respectively. The obtained flyer impact velocity, the particle velocity at the sample-LiF interface, and the wave velocity in the sample coupled with the known shock response of the flyer (Cu, 2024Al, and PMMA) and the LiF optical window [28,44] enabled us to determine the Hugoniot state ($P - V - u_p$ data) of the Ce-5wt. %La alloy

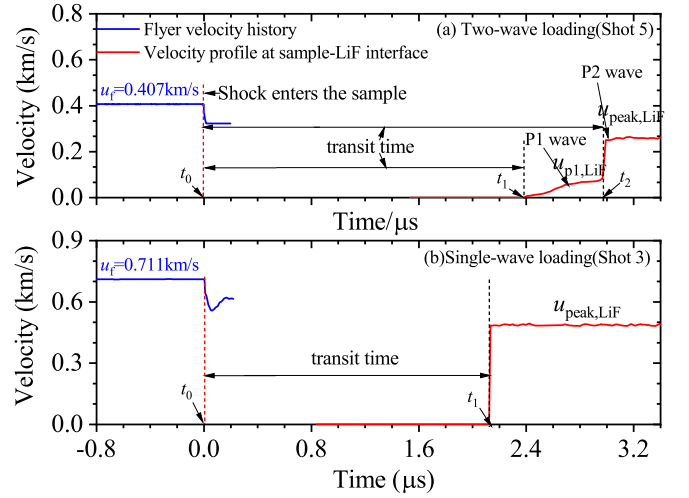


FIG. 3. The flyer velocity history and particle velocity profile at the sample-LiF interface for two different loading cases. (a) The measured result in shot 5 with two-wave loadings (the P1 wave and P2 wave). (b) The measured result in shot 3 with single-wave loading. The value of u_f is the impact velocity of the flyer on the sample, t_0 represents the time of the shock entering the sample, and t_1 and t_2 are the times of the shock arrivals at the sample-LiF interface.

by impedance matching methods and wave profile analysis. The Hugoniot parameters and densities of the Cu, 2024Al, PMMA and LiF used in the impedance matching calculations and wave profile analysis are shown in Table I.

According to the wave profile analysis method presented by Asay *et al.* [45], the differential relations between the changes in the particle velocity and the pressure of the LiF window ($du_{p,LiF}$ and dp_{LiF}) and the *in situ* values in the sample (du_p and dp) are given as

$$\begin{aligned} du_p &= \frac{1}{2} \left(du_{p,LiF} + \frac{dp_{LiF}}{\rho_0 u_s} \right) \\ dp &= \frac{1}{2} (dp_{LiF} + \rho_0 u_s du_{p,LiF}), \end{aligned} \quad (1)$$

where ρ_0 is the initial density of the Ce-5wt. %La alloy sample before a pressure increment and u_s is the Lagrangian wave velocity in the Ce-5wt. %La sample, corresponding to a pressure increment in the profile.

TABLE I. The Hugoniot parameters and densities of the Cu, 2024 Al, PMMA impactors and LiF window used in the impedance matching calculations and wave profile analysis. Note: C_0 and S are the fitted parameters in the linear relation of $u_s = C_0 + Su_p$. Here u_s and u_p are shock velocity and particle velocity, respectively.

Material	Hugoniot parameter			Reference
	Density(g/cm ³)	C_0 (km/s)	S	
Cu	8.933	3.933	1.50	Ref. [28]
2024Al	2.784	5.33	1.34	Ref. [44]
PMMA	1.18	2.58	1.53	Ref. [44]
LiF	2.64	5.15	1.35	Ref. [44]

The density states in the sample can be determined from the in-situ pressure histories in the sample, which are given as,

$$de = \frac{dp}{\rho_0 u_S^2}, \quad (2)$$

where e is the engineering strain, defined as $e = 1 - \rho_0/\rho$ and with a value of zero for the initial state (i.e., $e_0 = 0$).

Under the single-wave loading case [see Fig. 3(b)], the pressure (p_{peak}), particle velocity ($u_{p,\text{peak}}$), and compressed density (ρ_{peak}) corresponding to the peak loading state can be determined by Eqs. (1) and (2) coupled with the measured wave velocity (u_S) and sample-LiF interface particle velocity ($u_{\text{peak,LiF}}$), which are given as

$$\begin{aligned} u_{p,\text{peak}} &= \frac{1}{2} \left(u_{\text{peak,LiF}} + \frac{p_{\text{peak,LiF}}}{\rho_0 u_S} \right) \\ p_{\text{peak}} &= \frac{1}{2} (p_{\text{peak,LiF}} + \rho_0 u_S u_{\text{peak,LiF}}) \\ \rho_{\text{peak}} &= \frac{\rho_0}{1 - \frac{p_{\text{peak}}}{\rho_0 u_S^2}}, \end{aligned} \quad (3)$$

where $p_{\text{peak,LiF}}$ is the peak pressure in the LiF window under shock loading and is calculated using the formula of $p_{\text{peak,LiF}} = \rho_{0,\text{LiF}}(C_{0,\text{LiF}} + S_{\text{LiF}} u_{\text{peak,LiF}}) u_{\text{peak,LiF}}$ according to its Hugoniot parameters of $C_{0,\text{LiF}}$ and S_{LiF} and the measured $u_{\text{peak,LiF}}$.

Under the two-wave loading case [see Fig. 3(a)], the data processing includes two steps. Firstly, according to the measured wave velocity ($u_{S,P1}$) for the P1 wave and sample-LiF interface particle velocity ($u_{p1,\text{LiF}}$), we can obtain the pressure (p_{PT}), particle velocity ($u_{p,PT}$), and compressed density (ρ_{PT}) corresponding to the PT threshold state using Eqs. (1) and (2), which are given as

$$\begin{aligned} u_{p,PT} &= \frac{1}{2} \left(u_{p1,\text{LiF}} + \frac{p_{1,\text{LiF}}}{\rho_0 u_{S,P1}} \right) \\ p_{PT} &= \frac{1}{2} (p_{1,\text{LiF}} + \rho_0 u_{S,P1} u_{p1,\text{LiF}}) \\ \rho_{PT} &= \frac{\rho_0}{1 - \frac{p_{PT}}{\rho_0 u_{S,P1}^2}}, \end{aligned} \quad (4)$$

where $p_{1,\text{LiF}} = \rho_{0,\text{LiF}}(C_{0,\text{LiF}} + S_{\text{LiF}} u_{p1,\text{LiF}}) u_{p1,\text{LiF}}$ is the first-shock pressure in the LiF window under P1 wave loading. Secondly, for the following P2 wave loading, the corresponding pressure (p_{peak}), particle velocity ($u_{p,\text{peak}}$), and compressed density (ρ_{peak}) can be determined by integrating Eqs. (1) and (2) starting from the PT threshold state of the sample and the first-shocked state of the LiF window, which are given as

$$\begin{aligned} u_{p,\text{peak}} &= u_{p,PT} + \frac{1}{2} (u_{\text{peak,LiF}} - u_{p1,\text{LiF}}) \\ &\quad + \frac{1}{2\rho_{PT} u_{S,P2}} (p_{\text{peak,LiF}} - p_{1,\text{LiF}}) \\ p_{\text{peak}} &= p_{PT} + \frac{1}{2} (p_{\text{peak,LiF}} - p_{1,\text{LiF}}) \\ &\quad + \frac{1}{2} \rho_{PT} u_{S,P2} (u_{\text{peak,LiF}} - u_{p1,\text{LiF}}) \end{aligned}$$

$$\rho_{\text{peak}} = \frac{1}{\frac{1}{\rho_{PT}} - \frac{p_{\text{peak}} - p_{PT}}{\rho_{PT}^2 u_{S,P2}^2}}, \quad (5)$$

where $u_{\text{peak,LiF}}$ is the particle velocity corresponding to the second plateau of the sample-LiF interface particle velocity profile [see Fig. 3(a)], $p_{\text{peak,LiF}}$ is the shock pressure in the LiF window under the P2 wave loading and is obtained using the Hugoniot parameters $C_{0,\text{LiF}}$ and S_{LiF} and the measured $u_{\text{peak,LiF}}$, and $u_{S,P2}$ is the Lagrangian wave velocity for the P2 wave.

In addition, both for the single-wave loading and the P2 wave loading in the two-wave case, the peak states can also be determined using the standard impedance matching methods coupled with the measured flyer impacting velocity and wave velocity in the sample and the Hugoniot parameters of the flyer material, which can be cross-checked with the results from wave profile analysis. It is notable that the initial state values used in the impedance matching calculations, including the initial pressure, density, and particle velocity, are different for the single-wave loading and the P2 wave loading under the two-wave case. For single-wave loading, the used values of the initial pressure and particle velocity are zero and the used initial density is 6.693 g/cm³. For the P2 wave loading under the two-wave case, the used values of the initial pressure, particle velocity, and density are p_{PT} , $u_{p,PT}$, and ρ_{PT} , respectively, which need to be determined in advance by wave profile analysis.

III. RESULTS AND DISCUSSIONS

A. PT observations and PT threshold pressure determinations

Using the experimental method described in Sec. II, a total of seven experimental shots were performed with flyer impact velocities in the range of 0.364–1.527 km/s and the resulting peak pressures were determined to be in the range of 0.995–20.01 GPa. Relevant experimental parameters and measured results for shock compression experiments of the Ce-5wt. % La alloy are shown in Table II. Figure 4 shows the evolution of the measured particle velocity profiles at the sample-LiF interface with various peak loading pressures and flyer impact velocities. Wave profile measurements, including velocity and pressure profiles, can provide important information on the PTs of materials of interest under shock compression [7,11,46]. It can be clearly observed that the wave configuration changes from single-wave to two-wave, and then to single-wave again with an increase in the peak loading pressure. For shot 7 with the lowest peak pressure of $P_{\text{peak}} = 0.995$ GPa, a single-wave ramp wave loading is observed at the PMMA flyer velocity of 0.364 km/s. Such ramp wave loading is remarkably different from a shock jump and can be considered to be an isentropic compression process according to the result obtained for pure Ce by El'kin *et al.* [47]. When the P_{peak} increases and reaches 2.487 GPa with a flyer (2024A1) velocity of 0.420 km/s (shot 6) and 3.251 GPa with a flyer (Cu) velocity of 0.407 km/s (shot 5), respectively, the compression waves in the Ce-5wt. %La alloy split into two waves, a ramp wave (P1 wave) followed by a slow shock wave (P2 wave), which is a typical shock-jump characteristic. Thus, for the loading conditions of shots

TABLE II. Relevant experimental parameters and measured results for shock compression experiments of the Ce-5%wt.La alloy. The uncertainties are show in the parentheses.

Experiments	Impactor		Sample		Window		Impacting velocity u_f (km/s)	Phase transition state in the sample					Peak state in the sample		
	Material	Thickness (mm)	Material	Thickness (mm)	Material	Thickness (mm)		$u_{s,p1}$ (km/s)	$u_{p,PT}$ (km/s)	ρ_{PT} (g/cm ³)	P_{PT} (GPa)	$u_{s,p2}$ (km/s)	$u_{p,peak}$ (km/s)	ρ_{peak} (g/cm ³)	P_{peak} (GPa)
Shot 1	Cu	4.5	Ce-5%wt.La	4.017	LiF	12.0	1.527	–	–	–	–	2.863 (0.057)	1.044 (0.023)	10.54 (0.215)	20.01 (0.328)
Shot 2	Cu	4.5	Ce-5%wt.La	4.018	LiF	12.0	0.810	–	–	–	–	2.042 (0.039)	0.596 (0.013)	9.449 (0.193)	8.140 (0.157)
Shot 3	Cu	4.5	Ce-5%wt.La	4.109	LiF	12.0	0.711	–	–	–	–	1.934 (0.036)	0.528 (0.012)	9.205 (0.188)	6.832 (0.127)
Shot 4	Cu	4.5	Ce-5%wt.La	4.016	LiF	12.0	0.578	–	–	–	–	1.757 (0.038)	0.438 (0.009)	8.914 (0.182)	5.148 (0.101)
Shot 5	Cu	4.5	Ce-5%wt.La	4.108	LiF	12.0	0.407	1.728 (0.031)	0.0865 (0.002)	7.045 (0.146)	1.000 (0.023)	1.387 (0.026)	0.317 (0.007)	8.449 (0.174)	3.251 (0.103)
Shot 6	2024Al	6.0	Ce-5%wt.La	3.050	LiF	12.0	0.402	1.725 (0.033)	0.0864 (0.002)	7.045 (0.144)	0.997 (0.022)	1.218 (0.023)	0.260 (0.005)	8.216 (0.170)	2.487 (0.108)
Shot 7	PMMA	6.0	Ce-5%wt.La	3.926	LiF	12.0	0.364	–	–	–	–	1.723 (0.030)	0.0863 (0.002)	7.045 (0.138)	0.995 (0.026)

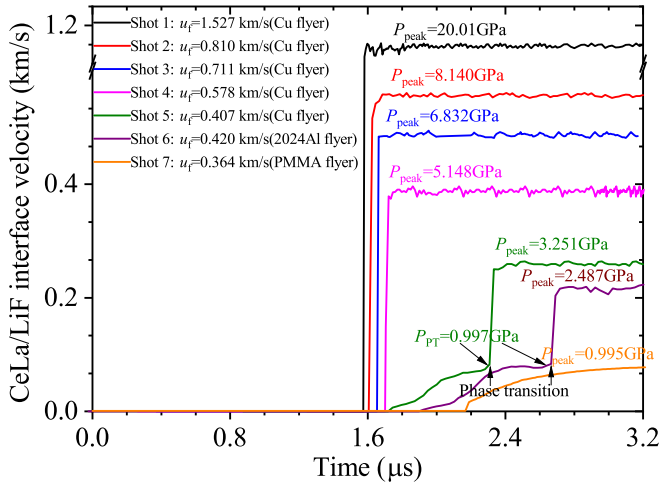


FIG. 4. The evolution of the measured particle velocity profiles at the sample-LiF interface with the peak loading pressure. Note that the signal is shifted along the time axis for different shots. P_{PT} and P_{peak} represent the PT threshold pressure and peak loading pressure, respectively.

5 and 6, a two-wave configuration with the participation of isentropic and shock waves is realized [47], similar to the findings in shock compression experiments for pure Ce in the low pressure $\gamma \rightarrow \alpha$ PT regime [7,11]. Further analysis shows that the P1 wave velocities in both shots 5 and 6 are found to have close values of $u_{s,P1} \cong 1.728$ km/s, although the peak loading pressures of these two shots are different. The wave velocities are markedly lower than the ambient longitudinal sound velocity of the Ce-5wt. %La alloy with a value of 2.368 km/s, showing that the formation of the two-wave particle velocity profiles is caused by the shock-induced $\gamma \rightarrow \alpha$ PT of the Ce-5wt. %La alloy but not the elastic-to-plastic transition. Under the two-wave loading condition, the P1 phase precursor wave first isentropically compressed the Ce-5wt. %La alloy into the PT threshold state and the following P2 shock wave then drove the sample to transform from the γ phase to the denser α phase. Thus, the observed compression wave splitting and formation of the two-wave structure can provide essential information and convincing evidence for analyzing the PT behavior of the dynamically compressed Ce-5wt. %La alloy. Using the obtained two-wave particle velocity profiles together with the P1 wave velocity, we can deduce the PT threshold pressure, P_{PT} , of the Ce-5wt. %La alloy to be 0.997 GPa based on wave profile analysis, a value slightly higher than the peak loading pressure of shot 7. In Fig. 4, we can also see that when the P_{peak} further climbs up to 5.148 GPa or higher in shots 1–4, the two-wave structure disappears and a single-wave shock jump is observed, which provides evidence that the $\gamma \rightarrow \alpha$ PT regime end pressure of the Ce-5wt. %La alloy is not beyond 5.148 GPa, since the formation of the single-shock wavefront is only possible in the pressure range exceeding the PT completion pressure [47]. Thus, the obtained particle velocity profiles at the sample-LiF interface clearly show the occurrence of the $\gamma \rightarrow \alpha$ PT of the dynamically compressed Ce-5wt. %La alloy when the peak loading pressure P_{peak} is in the range of 0.997 ~ 5.148 GPa. Furthermore, it is notable that in shots

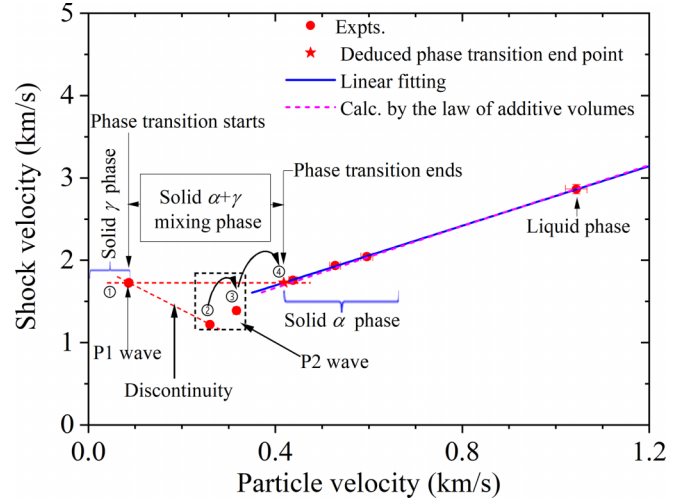


FIG. 5. The shock-wave velocity vs particle velocity for the Ce-5wt. %La alloy. The red solid circle and star represent our measured data and the deduced phase transition endpoint, respectively. The blue solid line is the linear fitting result using the experimental $u_s - u_p$ data for the Ce-5wt. %La alloy. The magenta dashed line is calculated using the Hugoniot parameters for pure Ce and La by the law of additive volumes of ideal mixtures.

5 and 6, when the P_{peak} reaches 3.251 and 2.487 GPa, respectively, although the P2 wave profile and corresponding wave velocity ($u_{s,P2}$) are different from the P1 wave profile and velocity ($u_{s,P1}$), the critical pressures required for PT activation are almost the same, showing that the PT pressure of the dynamically compressed Ce-5wt. %La alloy is almost independent of the peak state achieved in our considered pressure ranges.

B. Volume collapse and PT region determinations

Using the plate-impact shock loading technique, the thermodynamic spaces achieved in our experiments cover a range from the solid γ phase to the α phase and then to the liquid phase, providing essential information for locating the phase boundary and determining the PT regime of the dynamically compressed Ce-5wt. %La alloy. Figure 5 shows the measured data of the shock wave velocity (u_s) vs particle velocity (u_p) for the Ce-5wt. %La alloy. When the particle velocity reaches ~ 0.087 km/s or lower, the Ce-5wt. %La alloy is located in the solid γ phase region and no PT occurs since only a single ramp wave is observed (see shot 7 in Fig. 4). When the particle velocity exceeds ~ 0.087 km/s and is lower than ~ 0.438 km/s, the shock-induced $\gamma \rightarrow \alpha$ PT of the Ce-5wt. %La alloy takes place and a discontinuity is clearly observed in the $u_s - u_p$ plane (see ① \rightarrow ② in Fig. 5). This discontinuity can be attributed to the compression wave splitting and the formation of the two-wave structure when the PT occurs because the two waves propagate in the sample at different wave speeds, i.e., $u_{s,P1}$ for the P1 wave and $u_{s,P2}$ for the P2 wave (see shots 5 and 6 in Fig. 4). When the PT occurs in our experiments, the P1 wave speed ($u_{s,P1}$) is found to basically maintain a constant value of 1.728 km/s but the P2 wave speed ($u_{s,P2}$) gradually rises with the increase in the peak loading pressure (see ② \rightarrow ④ in Fig. 5). When the particle velocity reaches ~ 0.438

km/s or even higher, the thermodynamic spaces contain both the solid α phase and the liquid regime, and the obtained $u_s - u_p$ data in both phases are found to be approximately located on one line, which has a linear fitting relation of $u_s = 0.971 + 1.810u_p$. Note that in our experiments, the achieved highest-pressure state, i.e., shot 1, is in the liquid phase regime due to the occurrence of shock melting, which is validated by our reverse-impact sound velocity measurement and will be described in another manuscript. The obtained $u_s - u_p$ linear relation in the α and liquid phase regimes provides a hard-won opportunity to accurately locate the PT end state by extrapolating the $u_s - u_p$ fitting line, providing a particle velocity value of ~ 0.418 km/s (see point ④ in Fig. 5). At the PT end state, the P2 wave catches up with the P1 wave (i.e., $u_s = u_{s,P1} = u_{s,P2} = 1.728$ km/s), resulting in the disappearance of the two-wave structure and the formation of single-wave shock loading. Therefore, the PT end pressure can be determined to be ~ 4.835 GPa using the formula $P = \rho_0 u_s u_p$, where ρ_0 is the initial density of the Ce-5wt. %La alloy, and $u_s = 1.728$ km/s and $u_p = 0.418$ km/s are the shock wave velocity and particle velocity at the PT end state, respectively. The obtained PT end pressure is consistent with direct measurements from the particle velocity profile analysis (< 5.148 GPa). According to the deduced particle velocity at the PT end state, the density of the Ce-5wt. %La alloy in the denser α phase at the pressure of ~ 4.835 GPa can be also calculated as $\rho \cong 8.825$ g/cm³ using the formula $\rho = \rho_0 u_s / (u_s - u_p)$. Thus, based on the measured $u_s - u_p$ data, we can accurately locate the phase boundary and determine the PT regime of the Ce-5wt. %La alloy under dynamical compression in the range of 0.997–4.835 GPa and 7.045–8.825 g/cm³. By defining the volume compression from the γ phase to the α phase as $\Delta V_{\gamma \rightarrow \alpha} / V_\gamma = 1 - \rho_\gamma / \rho_\alpha$, a large volume collapse of $\sim 20\%$ was found when the Ce-5wt. %La alloy transformed from the γ phase with a density of $\rho_\gamma \cong 7.045$ g/cm³ at a pressure of 0.997 GPa to the α phase with a density of $\rho_\alpha \cong 8.825$ g/cm³ at a pressure of ~ 4.835 GPa. Such a large volume collapse under shock compression was previously observed in pure Ce [7] and it was considered to be responsible for the splitting of the shock front and the formation of a two- or multiwave structure when PT takes place [11].

Figure 6 shows the measured pressure (P) vs volume (V) data together with the calculated $P - V$ curves derived from the experimentally obtained $u_s - u_p$ linear fitting relation. The Rayleigh line determined by the initial and PT threshold states is also shown in Fig. 6, while its slope, $k = (P_{PT} - P_0) / (V_{PT} - V_0)$, is associated with the velocity of the P1 wave, i.e., $u_{s,P1} = V_0(-k)^{1/2}$, where (P_0, V_0) and (P_{PT}, V_{PT}) are the pressure and volume at the initial and PT threshold states, respectively. According to the Rankine-Hugoniot (RH) relations [48], for the P2 wave loading, its wave speed is determined by the PT threshold state and peak loading state as $u_{s,P2} = u_{s,P1} + V_{PT} \{ [(P_{\text{peak}} - P_{PT}) / (V_{PT} - V_{\text{peak}})]^{1/2} - [(P_{PT} - P_0) / (V_0 - V_{PT})]^{1/2} \}$ since the PT threshold state is the P2 wave's initial state. Considering the relation of $[(P_{\text{peak}} - P_{PT}) / (V_{PT} - V_{\text{peak}})]^{1/2} = [(P_{PT} - P_0) / (V_0 - V_{PT})]^{1/2}$ and the result $u_{s,P1} = u_{s,P2}$, when the two-wave structure disappears, we can also locate the PT end state of dynamically compressed Ce-5wt. %La alloy using the

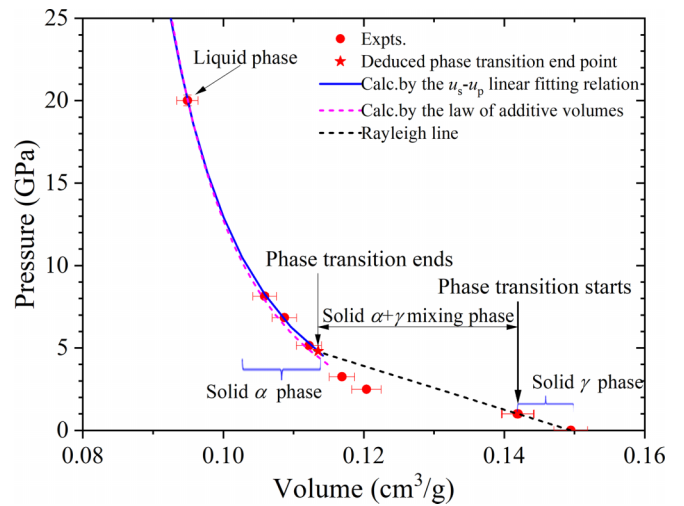


FIG. 6. Shock pressure vs volume for the Ce-5wt. %La alloy. The red solid circle and red solid star represent our measured data and deduced phase transition endpoint, respectively. The blue solid and magenta dashed lines are calculated by the experimental $u_s - u_p$ linear fitting relation and by the law of additive volumes of ideal mixtures. The black dashed line is the Rayleigh line determined from the initial and PT threshold states.

intersection between the Rayleigh line and the $P - V$ curve derived from the experimentally obtained $u_s - u_p$ linear fitting relation (see the red solid star in the Figure 6), which gives a pressure of 4.808 GPa, a density of $\rho_\gamma \cong 8.814$ g/cm³, and a volume collapse of $\sim 20\%$. These values together with the computed PT regime of 0.997–4.808 GPa and 7.045–8.814 g/cm³ are consistent with the calculation of 0.997–4.835 GPa and 7.045–8.825 g/cm³ deduced from the $u_s - u_p$ data.

The experimentally obtained $u_s - u_p$ and $P - V$ data of the Ce-5wt.%La alloy under shock compression provided a good opportunity for evaluating the law of additive volumes of ideal mixtures [49,50]. The law of additive volumes is a pressure mixing rule, which can be used to obtain the EOS of a mixture from the data of pure materials under certain conditions [51]. In order to evaluate its applicability to Ce-La alloy, we calculated the $u_s - u_p$ and $P - V$ data of the Ce-5wt.%La alloy in a pressure range of 4–25 GPa, spanning from α phase to the liquid phase, based on the law of additive volumes of ideal mixtures together with the available fitted Hugoniot parameters, C_0 and S , of pure Ce at the pressure of 4–48 GPa and La at the pressure of 5–22.5 GPa [41] and the calculated results are plotted in Figs. 5 and 6 for comparisons with the experiments. It is notable that a basic assumption needs to be satisfied when calculating the Hugoniot of the Ce-La alloy from the values of pure Ce and La using the law of additive volumes. The assumption is that when the Ce-La alloy is shock compressed no chemical reaction occurs between the Ce and La and the Ce-La alloy can be regarded as an ideal mixture of Ce and La [49,50]. As a result, when the Ce-La alloy is shock compressed the Ce and La of the mixture will be compressed along their own Hugoniot and then achieve an equilibrium pressure [49]. The Appendix shows the details of applying the law of additive volumes to calculate the Hugoniot of Ca-La from values of pure Ce and La and Table III lists the

TABLE III. The Hugoniot parameters of pure Ce, La, and Ce-5%wt.La alloy.

Material	Hugoniot parameter		Pressure range (GPa)	Reference
	C_0 (km/s)	S		
Ce	0.87	1.90	$4 < P < 48$	Ref. [41]
La	2.05	1.02	$5 < P < 22.5$	Ref. [41]
Ce-5%wt.La	0.971	1.81	$4.835 < P < 20.01$	This work

Hugoniot parameters of pure Ce, La, and Ce-5%wt.La alloy. From Figs. 5 and 6, it can be clearly seen that the calculations are in good agreement with the experimental data of the Ce-5wt.%La alloy, showing that the law of additive volumes of ideal mixtures is suitable for the Ce-5wt.%La alloy in the thermodynamic regime from the α phase to the liquid phase. This observation is valuable for us in using available shock wave data for pure Ce and La to predict the shock response of Ce-La alloys with different La additions when data is not available.

C. Effects of La additives on the thermodynamic behavior of Ce

By varying the atomic percentage of the La additives in the range of 0–6%, Gschneidner *et al.* [43] studied the $\gamma \rightarrow \alpha$ transformation of Ce-La alloys under static compression with a simple piston and cylinder device using glycerin as the pressure transmitting medium [43]. The PT pressure at 296 K was determined to be 0.97 GPa for Ce_{95%}La_{5%}, where the subscript represents the atomic percentage (note that the atomic percentage here is approximately equal to the weight percent due to the very close molar mass between Ce and La). Their experimental information indicated that La additives raised the $\gamma \rightarrow \alpha$ transformation pressure of pure Ce to an amplitude of ~ 0.4 kbar/at. % La impurity [43,52], which can be satisfactorily accounted for by an extension of the Ramirez-Falicov theory [53]. The recent ARPES experiments together with theoretical calculations within the scenario of the KVC model demonstrated that La doping in Ce weakens the $f - c$ hybridization effect and suppressed the $\gamma \rightarrow \alpha$ phase transition of Ce, resulting in greater PT pressure at room temperature [54]. Because of the lack of shock wave data, however, these results were limited to static compression at room temperature. Thus, our experimental Hugoniot data provide a unique opportunity to examine the effects of a few La additives on the thermodynamic behavior of Ce under dynamical shock compression. Up to now, there have been a large number of experimental and theoretical studies aiming at the $\gamma \rightarrow \alpha$ PT of Ce under pressure [3,5–8,11,21,22,33,40,41,55–62]. The PT threshold pressure of dynamically compressed Ce has been experimentally determined to be 0.76 GPa by Pavlovskii *et al.* [11] using explosive driven shock loading together with a pressure profile measurement and to be 0.92 GPa by Jensen and Cherne [7] using multiple gun driven shock loading together with a particle velocity profile measurement [7,11]. For the PT threshold pressure, a large difference of $\sim 21\%$ is found between the experiments of Pavlovskii *et al.* [11] and Jensen and Cherne [7], while the former was found to be in good agreement with the calculated results of 0.73 GPa by Elkin *et al.* [47,57] using a multiphase EOS. Compared with the

results for pure Ce from Pavlovskii *et al.* [11] and Jensen and Cherne [7], our shock compression experiments reveal that 5wt.% La additives raised the $\gamma \rightarrow \alpha$ transformation pressure of Ce to $\sim 31\%$ and $\sim 8.4\%$, respectively, showing that La additives might play an important role in the PT kinetics of shock-compressed Ce-La alloys. The La additives inducing an increase in the $\gamma \rightarrow \alpha$ transformation pressure of Ce under shock compression in our experiment is consistent with the static experiments of Gschneidner *et al.* [43] but the obtained PT threshold pressure (0.997 GPa) is slightly higher than their static experimental value (0.97 GPa) [43]. This higher threshold PT pressure value might be attributed to the fact that the isentropic compression realized in our experiment results in a slightly higher temperature than the room temperature maintained during static compression.

In order to further analyze the effects of La additions on the shock response of Ce, we performed comparisons between our experimental results for the Ce-5wt.%La alloy and the available shock wave experimental data for pure Ce and La both in the $u_s - u_p$ and $P - V$ spaces with the pressure range of [0, 25] GPa [5,7,8,11,41], as shown in Fig. 7. Note that in Fig. 7, for clarity, we use lines to represent the results for pure Ce and La in Ref. [41], which were obtained based on the linear fitting of experimentally determined $u_s - u_p$ data. A summary table gathering the various results from Ce and Ce-La experiments is shown in Table IV. Furthermore, we use the law of additive volumes to predict the Hugoniot of the Ce-La alloys with three higher La additions (25wt.%, 50wt.%, and 75wt.%, see Fig. 7). From the $u_s - u_p$ space, we can see the results for the Ce-La alloy located between the data for pure Ce and La, showing that La additions cause an increase in the parameter C_0 and a decrease in S , where C_0 and S are the fitting values of the $u_s - u_p$ linear relation of $u_s = C_0 + Su_p$. With the increase of the La additions, the $u_s - u_p$ lines of the Ce-La alloys gradually approach that of pure La. From the $P - V$ space, we can see that the results of the Ce-La alloy are also located between the data of the pure Ce and La, revealing that the La additions decrease the compressibility with respect to pure Ce. This compressibility decrease can be attributed to the “harder” Hugoniot of La compared with Ce, especially in the low-pressure region. With the increase in the La additions, the $P - V$ curve of the Ce-La alloys also gradually approaches that of pure La. Although the shock Hugoniot of Ce was affected by La additions, due to very few La additions in our experiments (5wt.%), both the $u_s - u_p$ and $P - V$ results of the Ce-5wt.%La alloy are very close to those of pure Ce and only a small difference can be observed between the Ce-5wt.%La and Ce. Meanwhile, the difference becomes smaller and smaller with the increase of the shock (or particle) velocity and shock pressure.

TABLE IV. Summary of various results for dynamically compressed Ce and Ce-5%wt.La. The uncertainties are shown in the parentheses.

Material		Phase transition state				Peak state				
		$u_{S,P1}$ (km/s)	$u_{p,PT}$ (km/s)	ρ_{PT} (g/cm ³)	P_{PT} (GPa)	$u_{S,P2}$ (km/s)	$u_{p,peak}$ (km/s)	ρ_{peak} (g/cm ³)	P_{peak} (GPa)	
Ce-5% wt.La	Experiment	–	–	–	–	2.863 (0.057)	1.044 (0.023)	10.54 (0.215)	20.01 (0.328)	This work
		–	–	–	–	2.042 (0.039)	0.596 (0.013)	9.449 (0.193)	8.140 (0.157)	
		–	–	–	–	1.934 (0.036)	0.528 (0.012)	9.205 (0.188)	6.832 (0.127)	
		–	–	–	–	1.757 (0.038)	0.438 (0.009)	8.914 (0.182)	5.148 (0.101)	
		1.728 (0.031)	0.0865 (0.002)	7.045 (0.146)	1.000 (0.023)	1.387 (0.026)	0.317 (0.007)	8.449 (0.174)	3.251 (0.103)	
		1.725 (0.033)	0.0864 (0.002)	7.045 (0.144)	0.997 (0.022)	1.218 (0.023)	0.260 (0.005)	8.216 (0.170)	2.487 (0.108)	
	–	–	–	–	1.723 (0.030)	0.0863 (0.002)	7.045 (0.138)	0.995 (0.026)		
Ce	Experiment	2.03	0.060	6.944	0.76	1.55	0.214	7.813	2.42	Ref. [11]
Ce	Experiment	1.599	0.086	7.072	0.920	0.942	0.213	8.174	1.767	Ref. [7]
	Calculation	–	–	7.065	0.70	–	–	8.395	1.84	
Ce	Calculation	–	–	–	0.75	–	–	–	–	Ref. [47]
Ce	Calculation	–	–	–	0.73	–	–	–	–	Ref. [57]
Ce	Experiment	–	–	–	–	1.723	0.451	–	5.20	Ref. [5]
		–	–	–	–	1.724	0.452	–	5.21	
		–	–	–	–	1.725	0.452	–	5.21	
		–	–	–	–	1.739	0.459	–	5.35	
		–	–	–	–	1.723	0.453	–	5.20	
		–	–	–	–	1.732	0.453	–	5.24	
		–	–	–	–	1.732	0.457	–	5.27	
		–	–	–	–	1.725	0.452	–	5.21	
		–	–	–	–	1.726	0.451	–	5.21	
		–	–	–	–	1.725	0.452	–	5.23	
Ce	Experiment	–	–	–	–	1.539 (0.027)	0.384 (0.002)	–	3.99 (0.060)	Ref. [8]
		–	–	–	–	1.299 (0.022)	0.307 (0.002)	–	2.70 (0.041)	
		–	–	–	–	1.818 (0.032)	0.509 (0.005)	–	6.26 (0.093)	
		–	–	–	–	2.579 (0.048)	0.885 (0.010)	–	15.25 (0.23)	
		–	–	–	–	1.800 (0.030)	0.482 (0.002)	–	5.800 (0.087)	
		–	–	–	–	2.043 (0.036)	0.598 (0.006)	–	8.170 (0.12)	
		–	–	–	–	2.100 (0.037)	0.684 (0.007)	–	9.610 (0.14)	
		–	–	–	–	2.270 (0.041)	0.730 (0.007)	–	11.08 (0.17)	
		–	–	–	–	2.429 (0.045)	0.790 (0.008)	–	12.83 (0.17)	
		–	–	–	–	2.421 (0.045)	0.752 (0.008)	–	12.17 (0.18)	
Ce	Experiment	–	–	–	–	2.377 (0.045)	0.791 (0.008)	–	12.57 (0.19)	Ref. [8]
		–	–	–	–	1.734 (0.022)	0.453 (0.002)	–	5.25 (0.053)	
		–	–	–	–	2.632 (0.030)	0.892 (0.005)	–	15.69 (0.12)	
		–	–	–	–	2.175 (0.060)	0.647 (0.005)	–	9.410 (0.19)	
		–	–	–	–	2.415 (0.020)	0.794 (0.005)	–	12.83 (0.10)	
		–	–	–	–	2.463 (0.040)	0.819 (0.005)	–	13.48 (0.15)	
		–	–	–	–	0.955 (0.010)	0.228 (0.001)	–	1.880 (0.03)	
		–	–	–	–	2.745 (0.028)	0.985 (0.005)	–	18.08 (0.15)	
		–	–	–	–	0.925 (0.005)	0.219 (0.002)	–	1.683 (0.011)	
Ce	Experiment	–	–	–	–	1.57	0.39	8.99	4	Ref. [41]
		–	–	–	–	1.90	0.50	9.13	6	
		–	–	–	–	2.33	0.74	9.87	12	
		–	–	–	–	2.29	0.79	10.32	12	
		–	–	–	–	2.67	0.94	10.40	17	
		–	–	–	–	2.64	0.95	10.54	17	
		–	–	–	–	2.85	1.02	10.52	20	
		–	–	–	–	3.09	1.18	10.85	24	

IV. CONCLUSIONS

In conclusion, we have studied the shock response of Ce-5wt.%La alloy under dynamic compression up to 20 GPa using plate-impact shock experiments. A shock-induced volume collapse PT from γ to α was observed and the PT region

was determined to be within the range of [0.997, 4.835] GPa. The obtained PT threshold pressure in the Ce-5wt.%La alloy was found to be drastically different from that in pure Ce, showing that the few La additives have an important effect on the PT kinetics of dynamically compressed Ce. Based on the present $u_s - u_p$ and $P - V$ data, we have also examined

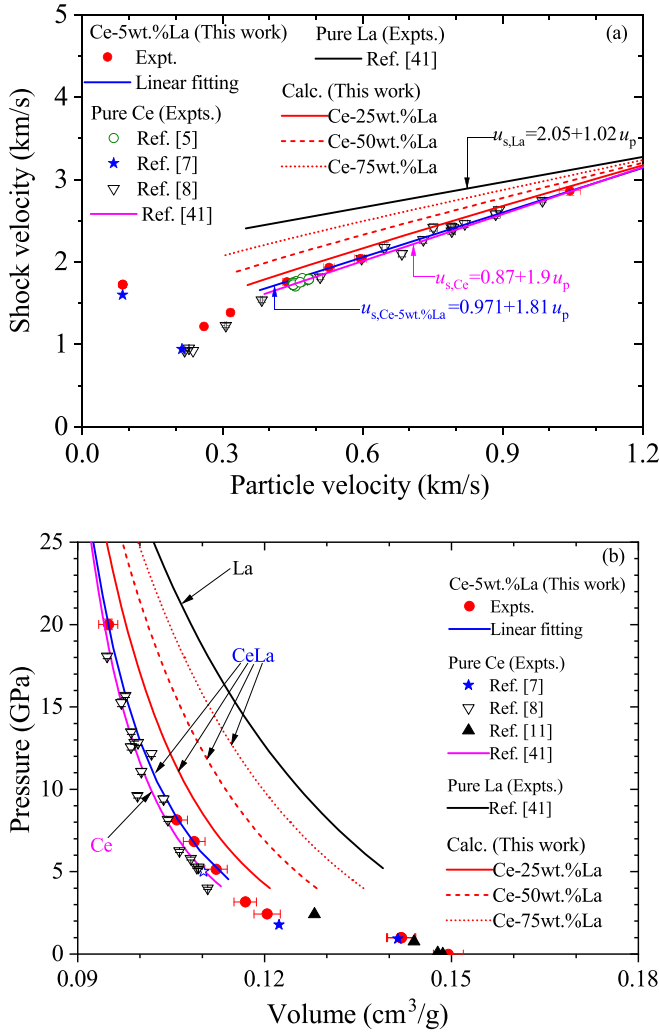


FIG. 7. A comparison of the Hugoniot data between the Ce-La alloy and pure Ce and La. (a) The $u_s - u_p$ data of the Ce-La alloys are compared with the available data for pure Ce and La [5,7,8,41]. (b) The $P - V$ data of the Ce-La alloys are compared with the available data for pure Ce and La [7,8,11,41]. The experimental results for pure Ce and La in Ref. [41] are shown by the solid magenta and black lines, respectively. The calculated results for three La additions of 25wt. %, 50wt. %, and 75wt. % by the law of additive volumes of ideal mixtures are also plotted for comparison.

and confirmed the effectiveness of the law of additive volumes of ideal mixtures for a Ce-La alloy system, which can provide useful information when experimental data for Ce-La alloys with arbitrary atomic percentages are not available. Our data and observations can provide essential information for understanding the multiphase properties and shock responses of dynamically compressed Ce and its alloys, and may have potential industrial applications in the synthesis of new materials at high pressure. Although the thermodynamic space of Ce-La alloys has been explored, our results obtained in shock experiments are macroscopic quantities and the changes in electronic structure under pressure cannot be directly observed. Because of the lack of direct electronic structure information under shock loading, except La additions raising the PT pressure in Ce, it is not clear whether the

underlying electronic picture under dynamical compression is also consistent with the available static ARPES experiment. Thus, direct measurements of microscopic information on electronic properties in Ce-La alloy under shock compression might be of considerable significance, which will be an important subject of future research.

ACKNOWLEDGMENTS

We thank the gas gun, diagnostic, and assembly teams for the experimental assistance. This work was supported by the National Natural Science Foundation of China (Grant No. 11872057) and the foundation of National Key Laboratory of Shock Wave and Detonation Physics, China Academy of Engineering Physics (Grant No. JCKYS2020212009).

APPENDIX: HUGONIOT CALCULATIONS BASED ON THE LAW OF ADDITIVE VOLUMES OF IDEAL-MIXTURE

The Hugoniot calculations of the Ce-La alloy were performed using the law of additive volumes of ideal-mixture [49–51] coupled with the Hugoniot parameters of the pure Ce and La [41]. According to the law of additive volumes of ideal-mixture, the pressure and volume of the Ce-La alloy under shock compression can be described as [49–51],

$$P_{Ce-La} = P_{Ce} = P_{La} \quad (A1)$$

$$V_{Ce-La} = (1 - x_{La})V_{Ce} + x_{La}V_{La}$$

where P and V are pressure and volume along the Hugoniot, respectively, x is the weight percent, and the subscripts represent the components of the mixture.

Using the well-known shock Hugoniot relation, the pressure and volume of pure Ce and La along their Hugoniot are calculated as

$$P_{Ce} = \rho_{0,Ce}(C_{0,Ce} + S_{Ce}u_{p,Ce})u_{p,Ce}$$

$$V_{Ce} = \frac{1}{\rho_{0,Ce}} \frac{C_{0,Ce} + S_{Ce}u_{p,Ce} - u_{p,Ce}}{C_{0,Ce} + S_{Ce}u_{p,Ce}}, \quad (A2)$$

$$P_{La} = \rho_{0,La}(C_{0,La} + S_{La}u_{p,La})u_{p,La}$$

$$V_{La} = \frac{1}{\rho_{0,La}} \frac{C_{0,La} + S_{La}u_{p,La} - u_{p,La}}{C_{0,La} + S_{La}u_{p,La}}, \quad (A3)$$

where ρ_0 and u_p are the initial density and particle velocity, respectively, and C_0 and S are the Hugoniot parameters.

Combining Eqs. (A1)–(A3), the pressure vs volume data along the Hugoniot of the Ce-La alloy can be obtained according to the following steps by changing pressure. The first step: calculate the particle velocity u_p and volume V of pure Ce and La at pressure of P using Eqs. (A2)–(A3). The second step: calculate the volume V of Ce-La alloy using Eq. (A1). Repeat these two steps when changing the pressure.

After obtaining the pressure vs volume data along the Hugoniot the resulting shock-velocity (u_s) vs particle velocity (u_p) data can be also calculated as

$$u_{p,Ce-La} = \sqrt{(P_{Ce-La} - P_0)(V_{0,Ce-La} - V_{Ce-La})} \quad (A4)$$

$$u_{s,Ce-La} = V_{0,Ce-La} \sqrt{\frac{P_{Ce-La} - P_0}{V_{0,Ce-La} - V_{Ce-La}}},$$

where $P_0 = 0$ is the initial pressure and $V_{0,Ce-La} = 1/\rho_{0,Ce-La}$ is the initial volume.

- [1] A. Fernandez-Pañella, M. Millot, D. E. Fratanduono, M. P. Desjarlais, S. Hamel, M. C. Marshall, D. J. Erskine, P. A. Sterne, S. Haan, T. R. Boehly, G. W. Collins, J. H. Eggert, and P. M. Celliers, Shock compression of liquid deuterium up to 1 TPa, *Phys. Rev. Lett.* **122**, 255702 (2019).
- [2] M. D. Knudson and M. P. Desjarlais, High-precision shock wave measurements of deuterium: Evaluation of exchange-correlation functionals at the molecular-to-atomic transition, *Phys. Rev. Lett.* **118**, 035501 (2017).
- [3] R. S. Hixson, B. M. La Lone, M. D. Staska, G. D. Stevens, W. D. Turley, and L. R. Veaser, Temperature measurements in cerium shocked from 8.4 to 23.5 GPa, *J. Appl. Phys.* **129**, 155106 (2021).
- [4] Z.-Q. Wang, Y.-J. Gu, Q.-F. Chen, Z.-G. Li, L. Liu, G.-J. Li, Y.-S. Lan, and X.-R. Chen, Equation of state measurements of dense krypton up to the insulator-metal transition regime: Evaluating the exchange-correlation functionals, *Phys. Rev. B* **103**, 014109 (2021).
- [5] B. J. Jensen, F. J. Cherne, and N. Velisavljevic, Dynamic experiments to study the $\alpha - \epsilon$ phase transition in cerium, *J. Appl. Phys.* **127**, 095901 (2020).
- [6] B. J. Jensen, T. M. Hartsfield, D. B. Holtkamp, F. J. Cherne, R. B. Corrow, T. E. Graves, and A. J. Iverson, Examining the high-pressure response and shock melting in cerium using optical pyrometry, *Phys. Rev. B* **102**, 214105 (2020).
- [7] B. J. Jensen and F. J. Cherne, Dynamic compression of cerium in the low-pressure $\gamma - \alpha$ region of the phase diagram, *J. Appl. Phys.* **112**, 013515 (2012).
- [8] B. J. Jensen, F. J. Cherne, J. C. Cooley, M. V. Zhernokletov, and A. E. Kovalev, Shock melting of cerium, *Phys. Rev. B* **81**, 214109 (2010).
- [9] A. V. Nikolaev and A. V. Tsvyashchenko, The puzzle of the $\gamma \rightarrow \alpha$ and other phase transitions in cerium, *Phys. Usp.* **55**, 657 (2012).
- [10] M. K. Wilkinson, H. R. Child, C. J. McHargue, W. C. Koehler, and E. O. Wollan, Neutron diffraction investigations of metallic cerium at low temperatures, *Phys. Rev.* **122**, 1409 (1961).
- [11] M. N. Pavlovskii, V. V. Komissarov, and A. R. Kutsar, Isomorphic $\gamma \rightarrow \alpha$ phase transition of cerium under shock compression, *Combust. Explos. Shock. Waves* **35**, 88 (1999).
- [12] O. B. Tsiok and L. G. Khvostantsev, Phase transitions in cerium at high pressures (up to 15 GPa) and high temperatures, *J. Exp. Theor. Phys.* **93**, 1245 (2001).
- [13] X.-G. Zhu, Y. Liu, Y.-W. Zhao, Y.-C. Wang, Y. Zhang, C. Lu, Y. Duan, D.-H. Xie, W. Feng, D. Jian, Y.-H. Wang, S.-Y. Tan, Q. Liu, W. Zhang, Y. Liu, L.-Z. Luo, X.-B. Luo, Q.-Y. Chen, H.-F. Song, and X.-C. Lai, Kondo scenario of the $\gamma - \alpha$ phase transition in single crystalline cerium thin films, *npj Quantum Mater.* **5**, 47 (2020).
- [14] D. R. Gustafson, J. D. McNutt, and L. O. Roellig, Positron annihilation in γ - and α -cerium, *Phys. Rev.* **183**, 435 (1969).
- [15] R. F. Gempel, D. R. Gustafson, and J. D. Willenberg, Investigation of the electronic structure of α' -cerium by angular-correlation studies of positron-annihilation radiation, *Phys. Rev. B* **5**, 2082 (1972).
- [16] U. Kornstädt, R. Lässer, and B. Lengeler, Investigation of the $\gamma - \alpha$ phase transition in cerium by Compton scattering, *Phys. Rev. B* **21**, 1898 (1980).
- [17] A. P. Murani, J. Reske, A. S. Ivanov, and P. Palleau, Evolution of the spin-orbit excitation across the $\gamma \rightarrow \alpha$ transition in Ce, *Phys. Rev. B* **65**, 094416 (2002).
- [18] A. P. Murani, S. J. Levett, and J. W. Taylor, Magnetic form factor of α -Ce: Towards understanding the magnetism of cerium, *Phys. Rev. Lett.* **95**, 256403 (2005).
- [19] W. E. Pickett, A. J. Freeman, and D. D. Koelling, Local-density-functional approach to the isostructural $\gamma - \alpha$ transition in cerium using the self-consistent linearized-augmented-plane-wave method, *Phys. Rev. B* **23**, 1266 (1981).
- [20] B. Johansson, The $\alpha - \gamma$ transition in cerium is a Mott transition, *Philos. Mag.* **30**, 469 (1974).
- [21] J. W. Allen and L. Z. Liu, α - γ transition in Ce. II. A detailed analysis of the Kondo volume-collapse model, *Phys. Rev. B* **46**, 5047 (1992).
- [22] J. W. Allen and R. M. Martin, Kondo volume collapse and the $\gamma \rightarrow \alpha$ transition in Cerium, *Phys. Rev. Lett.* **49**, 1106 (1982).
- [23] Y. Wu, Y. Fang, P. Li, Z. Xiao, H. Zheng, H. Yuan, C. Cao, Y.-f. Yang, and Y. Liu, Bandwidth-control orbital-selective delocalization of 4f electrons in epitaxial Ce films, *Nat. Commun.* **12**, 2520 (2021).
- [24] G.-J. Li, Z.-G. Li, Q.-F. Chen, Y.-J. Gu, W. Zhang, L. Liu, H.-Y. Geng, Z.-Q. Wang, Y.-S. Lan, Y. Hou, J.-Y. Dai, and X.-R. Chen, Multishock to quasi-isentropic compression of dense gaseous deuterium-helium mixtures up to 120 GPa: Probing the sound velocities relevant to planetary interiors, *Phys. Rev. Lett.* **126**, 075701 (2021).
- [25] L. Liu, Q.-F. Chen, Y.-J. Gu, W. Zhang, Z.-G. Li, C.-J. Li, Z.-Q. Wang, G.-J. Li, Y.-S. Lan, and X.-R. Chen, Measurement of multiple physical parameters of dense gaseous hydrogen-deuterium mixture under double-shock compression: Evaluating theoretical models from multiple views, *Appl. Phys. Lett.* **115**, 231905 (2019).
- [26] J. Tang, Y. J. Gu, Q. F. Chen, Z. G. Li, J. Zheng, C. J. Li, and J. T. Li, Multiple shock reverberation compression of dense Ne up to the warm dense regime: Evaluating the theoretical models, *Phys. Rev. B* **97**, 140101(R) (2018).
- [27] D. G. Hicks, T. R. Boehly, P. M. Celliers, J. H. Eggert, S. J. Moon, D. D. Meyerhofer, and G. W. Collins, Laser-driven single shock compression of fluid deuterium from 45 to 220 GPa, *Phys. Rev. B* **79**, 014112 (2009).
- [28] W. J. Nellis, A. C. Mitchell, and D. A. Young, Equation-of-state measurements for aluminum, copper, and tantalum in the pressure range 80–440 GPa (0.8–4.4 Mbar), *J. Appl. Phys.* **93**, 304 (2003).
- [29] W. J. Nellis, J. A. Moriarty, A. C. Mitchell, and N. C. Holmes, Equation of state of beryllium at shock pressures of 0.4–1.1 TPa (4–11 Mbar), *J. Appl. Phys.* **82**, 2225 (1997).
- [30] Y. Fei, C. T. Seagle, J. P. Townsend, C. A. McCoy, A. Boujibar, P. Driscoll, L. Shulenburg, and M. D. Furnish, Melting and density of MgSiO₃ determined by shock compression of bridgmanite to 1254 GPa, *Nat. Commun.* **12**, 876 (2021).
- [31] X. Liu, T. Mashimo, N. Kawai, T. Sano, and X. Zhou, Isotropic phase transition of single-crystal iron (Fe) under shock compression, *J. Appl. Phys.* **124**, 215101 (2018).
- [32] C. T. Adcock, O. Tschauner, E. M. Hausrath, A. Udry, S. N. Luo, Y. Cai, M. Ren, A. Lanzirrotti, M. Newville, M. Kunz, and C. Lin, Shock-transformation of whitlockite to merrillite and the implications for meteoritic phosphate, *Nat. Commun.* **8**, 14667 (2017).

- [33] W. J. Nellis, D. C. Hamilton, and A. C. Mitchell, Electrical conductivities of methane, benzene, and polybutene shock compressed to 60 GPa (600 kbar), *J. Chem. Phys.* **115**, 1015 (2001).
- [34] W. J. Nellis, S. T. Weir, and A. C. Mitchell, Minimum metallic conductivity of fluid hydrogen at 140 GPa (1.4 Mbar), *Phys. Rev. B* **59**, 3434 (1999).
- [35] D. W. Wheeler, The oxidation behaviour of Ce-5at.% La in air at ambient temperature, *Solid State Ionics* **313**, 22 (2017).
- [36] D. W. Wheeler and I. Khan, A Raman spectroscopy study of cerium oxide in a cerium-5wt.% lanthanum alloy, *Vib. Spectrosc.* **70**, 200 (2014).
- [37] D. W. Wheeler, J. Zekonyte, and R. J. K. Wood, Mechanical properties of cerium and a cerium-5wt% lanthanum alloy by nanoindentation and ultrasonic velocity measurements, *Materials Science and Engineering: A* **578**, 294 (2013).
- [38] D. W. Wheeler, J. Zekonyte, and R. J. K. Wood, Structure and mechanical properties of Ce-La alloys containing 3–10 wt. % La, *J. Nucl. Mater.* **543**, 152497 (2021).
- [39] F. E. Gibbs, D. L. Olson, and W. Hutchinson, Identification of a physical metallurgy surrogate for the plutonium-1 wt. % gallium alloy, *AIP Conf. Proc.* **532**, 98 (2000).
- [40] M. V. Zhernokletov, A. E. Kovalev, V. V. Komissarov, M. G. Novikov, M. A. Zocher, and F. J. Cherne, Measurement of sound velocities and shear strength of cerium under shock compression, *J. Phys.: Conf. Ser.* **121**, 072003 (2008).
- [41] W. J. Carter, J. N. Fritz, S. P. Marsh, and R. G. McQueen, Hugoniot equation of state of the lanthanides, *J. Phys. Chem. Solids* **36**, 741 (1975).
- [42] Z.-Y. Zeng, C.-E. Hu, Z.-G. Li, W. Zhang, and L.-C. Cai, High pressure phase transition of Ce-La alloy from first-principles calculations, *J. Alloys Compd.* **640**, 201 (2015).
- [43] K. A. Gschneidner, R. O. Elliott, and R. R. McDonald, Effects of alloying additions on the $\alpha \rightleftharpoons \gamma$ transformation of cerium: Part II. Effects of scandium, thorium and plutonium additions, *J. Phys. Chem. Solids* **23**, 1191 (1962).
- [44] T. S. Duffy and T. J. Ahrens, Dynamic compression of an Fe-Cr-Ni alloy to 80 GPa, *J. Appl. Phys.* **82**, 4259 (1997).
- [45] J. R. Asay, L. C. Chhabildas, and D. P. Dandekar, Shear strength of shock-loaded polycrystalline tungsten, *J. Appl. Phys.* **51**, 4774 (1980).
- [46] L. M. Barker and R. E. Hollenbach, Shock wave study of the $\alpha \leftrightarrow \epsilon$ phase transition in iron, *J. Appl. Phys.* **45**, 4872 (1974).
- [47] V. M. El'kin, E. A. Kozlov, E. V. Kakshina, and Y. S. Moreva, Equation of state and the dynamic compression of cerium in the range of the $\gamma - \alpha$ phase transition, *Phys. Metals Metallogr.* **101**, 208 (2006).
- [48] W. J. Nellis, A. C. Mitchell, M. van Thiel, G. J. Devine, R. J. Trainor, and N. Brown, Equation-of-state data for molecular hydrogen and deuterium at shock pressures in the range 2–76 GPa (20–760 kbar), *J. Chem. Phys.* **79**, 1480 (1983).
- [49] F. Q. Jing, *Introduction to Experimental Equation of State* (Science Press, Beijing, 1986).
- [50] H. Tan, *Experimental Shock Wave Physics* (National Defense Industry Press, Beijing, 2018).
- [51] R. J. Magyar and T. R. Mattsson, Mixing of equations of state for xenon-deuterium using density functional theory, *Phys. Plasmas* **20**, 032701 (2013).
- [52] B. Alascio, A. López, and C. F. E. Olmedo, Electronic phase transition in $\text{Ce}_{1-x}\text{La}_x$ alloys, *Phys. Rev. B* **7**, 4743 (1973).
- [53] R. Ramírez and M. Kiwi, Electronic phase transitions in $\text{Ce}_{1-x}\text{La}_x$ alloys, *Phys. Rev. Lett.* **28**, 344 (1972).
- [54] Y.-H. Wang, Y. Zhang, Y. Liu, X. Tan, C. Ma, Y.-C. Wang, Q. Zhang, D.-P. Yuan, D. Jian, J. Wu, C. Lai, X.-Y. Wang, X.-B. Luo, Q.-Y. Chen, W. Feng, Q. Liu, Q.-Q. Hao, Y. Liu, S.-Y. Tan, X.-G. Zhu *et al.*, Effect of $f - c$ hybridization on the $\gamma \rightarrow \alpha$ phase transition of cerium studied by lanthanum doping, *Chin. Phys. B* **31**, 087102 (2022).
- [55] C. W. Greeff, S. D. Crockett, and K. G. Honnell, Equation of state model for the $\gamma - \alpha$ transition in Ce, *AIP Conf. Proc.* **1979**, 030003 (2018).
- [56] M. J. Lipp, Z. Jenei, H. Cynn, Y. Kono, C. Park, C. Kenney-Benson, and W. J. Evans, Anomalous elastic properties across the γ to α volume collapse in cerium, *Nat. Commun.* **8**, 1198 (2017).
- [57] V. M. El'kin, V. N. Mikhaylov, A. V. Petrovtsev, and F. J. Cherne, Phase states of dynamically compressed cerium, *Phys. Rev. B* **84**, 094120 (2011).
- [58] F. Decremps, L. Belhadi, D. L. Farber, K. T. Moore, F. Occelli, M. Gauthier, A. Polian, D. Antonangeli, C. M. Aracne-Ruddle, and B. Amadon, Diffusionless $\gamma \rightleftharpoons \alpha$ phase transition in polycrystalline and single-crystal cerium, *Phys. Rev. Lett.* **106**, 065701 (2011).
- [59] D. Antonangeli, D. L. Farber, C. M. Aracne, D. G. Ruddle, J. Siebert, and B. P. Bonner, Kinetics of the isostructural γ to α transition in cerium investigated by ultrasonics, *High Press. Res.* **30**, 151 (2010).
- [60] M. J. Lipp, D. Jackson, H. Cynn, C. Aracne, W. J. Evans, and A. K. McMahan, Thermal signatures of the Kondo volume collapse in cerium, *Phys. Rev. Lett.* **101**, 165703 (2008).
- [61] V. A. Borisenok, V. G. Simakov, V. A. Volgin, V. M. Bel'skii, and M. V. Zhernokletov, Investigation of phase transformations in iron and cerium using a polyvinylidene fluoride pressure gauge, *Combust. Explos. Shock Waves* **43**, 476 (2007).
- [62] P. W. Bridgman, The compressibility and pressure coefficient of resistance of ten elements, *Proc. Am. Acad. Arts Sci.* **62**, 207 (1927).